Environmental Science Nano

ROYAL SOCIETY OF CHEMISTRY

PAPER

View Article Online
View Journal | View Issue

Cite this: *Environ. Sci.: Nano*, 2023, **10**, 1385

Interfacial interactions of humic acids with polystyrene nano-plastics in aqueous/ionic environments: a molecular dynamics exploration†

Prasad Rama, *[a] Julián A. Gallego-Urrea [b] and Zareen Abbas [a]

Plastics pose a serious threat to both marine and freshwater life after being discarded and broken down into smaller particles such as micro and nano-plastic particles. The nano-sized plastic particles are small enough in size and similar to surfaces of biological molecules, thereby potentially altering the intra-cellular interactions and their biological fate. In order to increase our understanding of the interactions among the molecules of natural organic matter and carboxylate functionalized polystyrene nano-plastics, we have performed a modelling study of the aquatic environment at different pH conditions using molecular dynamics (MD) simulations at an atomistic scale. Humic acids (HAs) are the most common constituents of natural organic matter, usually found in soil, water, and its sediments. As a proxy for humic acids, we have used Temple-Northeastern-Birmingham (TNB), an equivalent molecule to HA in its composition. We show that TNB molecules exhibit strong interactions with polystyrene (PS) nano-plastic particles at pH-4 but weak interaction at pH-7, whereas moderate interaction at pH-9 both in fresh and saltwater. The interaction between carboxylated polystyrene particles and TNB molecules is found to be counter-ion mediated and is enhanced in the presence of saltwater, *i.e.*, at 0.5 M NaCl electrolyte. An enhanced condensation of Na^+ counter-ions onto the surface of nano-plastics brings more water molecules to its interface, hence, enriching the hydrophilicity of nano-plastics. An ordered network structure of water molecules has also been observed at the interface of the PS-slab with an increase in pH of the aquatic environment, leading to a preferential alignment of water molecules, resulting in a strong hydration layer. This strong hydration layer also keeps the TNB molecules away from the vicinity of the PS-slab interface. The surface potential trends obtained from the MD simulations are in agreement with the measured zeta potential values showing that the surface charge density of PS nano-plastics increases with an increase in the pH of aquatic solutions. Hence, our simulations provide molecular-level insights into the phenomenon associated with the adsorption/accumulation of molecules of natural organic matter towards the nano-plastics and are helpful in understanding the formation of eco-corona on plastic nanoparticles.

Received 5th October 2022,
Accepted 10th March 2023

DOI: 10.1039/d2en00916a

rsc.li/es-nano

Environmental significance

Polystyrene is a widely used thermoplastic that ends up as plastic waste after being discarded and is carried to lakes/oceans, where they degrade into micro/nano-sized particles. The nano-sized plastic particles are small enough and similar to surfaces of biological molecules, thereby potentially altering intra-cellular interactions and their biological fate. The dissolved organic matter present in the lakes/oceans interacts with these nano-plastics and forms an eco-corona. The formation of eco-corona around the nano-plastics mainly occurs through hydrogen bonding, van der Waals forces, and hydrophobic and electrostatic interactions. Based on detailed atomistic level information gained by molecular dynamics, we have highlighted the fundamental mechanisms governing the interactions of organic molecules with PS-slab in pure and saltwater conditions at different pH values. The study highlights the influence of surface charge density of the nano-plastic in various aquatic conditions on its surface potential and surface hydration, which in turn affect the adsorption behaviour of humic acids (TNB molecules) onto its interface. Our simulation results can be very helpful in understanding the corona formation and plays a vital part in the ecotoxicity of these nano-plastics.

[a] *Department of Chemistry and Molecular Biology, University of Gothenburg, Gothenburg – 40530, Sweden. E-mail: prasad.rama@gu.se*
[b] *Department of Marine Science, University of Gothenburg, Gothenburg – 40530, Sweden*

† Electronic supplementary information (ESI) available: Data for radial number density distribution profiles of ion condensation at the interface of PS-slab, Donor–Acceptor distance for h-bonds formed at the PS-slab geometric interface were made available. See DOI: https://doi.org/10.1039/d2en00916a

1. Introduction

Polystyrene (PS) is a widely used plastic material as a result of its many applications, excellent physiochemical properties, as well as its low cost of production.[1] The applications of PS are numerous, ranging from plastic cups to additives in paints and cosmetics, which has led to PS of different sizes being widely spread as waste in the environment. Polystyrene nano-plastics can be functionalized with different functional groups to tailor their properties. Such properties include, for example, changes in electroactivity, adsorption to different materials, biological activity, light emission, and absorption.[2] With an increase in the wide usage of these plastic products globally, they eventually end up as plastic waste after being used and disposed into the environment. Lakes, streams, and rivers can act as receivers, sinks, and transporters of plastic pollution,[3] which finally ends up in the ocean. In an aqueous environment, the plastic material further breaks down into smaller pieces and eventually into nano-plastics (<100 nm in diameter)[4,5] due to their exposure to sunlight, oceanic waves, and living organisms present in water and the water itself.[6,7] Due to their unique surface-to-volume ratio, such nano-sized plastics exhibit potential biological impacts on aquatic living organisms.[8] Assessments of surface lake water report microplastic concentrations ranging from 0.21 to 34 000 particles per m^3.[9] Note that those are micro-plastic concentrations since quantifying NP in complex environmental matrices is still analytically challenging.

Natural organic matter (NOM) is a complex mixture of organic molecules that are usually found in water, soil, and sediments,[10,11] in the form of extracellular polymeric substances (DNA, proteins, carbohydrates, *etc.*) and humic substances (*e.g.*, humic and fulvic acids). These biomolecules interact with nano-plastics and encapsulate them to form a unique layered structure termed eco-corona, which can alter the physicochemical characteristics, interaction, fate, and effects of these plastic nanoparticles in the ecosystem.[12,13]

The interaction of nano-plastics in an aqueous environment with the biological fate of organisms depends on their size, shape, surface charge, and other properties.[8] The organic molecules of NOM may interact with the nano-plastic surface to form an eco-corona that can potentially modify the nature of nano-plastic interactions with the cell and organism surfaces and thereby its toxicity to aquatic life. The formation of eco-corona around the nano-plastics mainly occurs through hydrogen bonding, van der Waals forces, and hydrophobic and electrostatic interactions. There are numerous experimental studies reported in the literature on the interactions of nano-plastics with NOM in aquatic environments. For example, Shams *et al.*,[14] reported that polyethylene and polystyrene nano-plastics exhibit stronger interactions with NOM-coated surfaces in aquatic environments of monovalent and divalent salts, indicating that the fate and mobility of nano-plastics are governed by the interactions with NOM. Moreover, Saavedra *et al.*[15] demonstrated a study showing that the surface charge of nano-plastic can influence the formation of eco-corona and thereby its toxicity to zooplankton. Schultz *et al.*[16] studied the toxicity of 50 and 60 nm polystyrene nano-plastics with respect to the amine and carboxylated functionalized groups, elucidating that surface functionalization may change the nature of nano-plastic interactions with membranes and organelles, leading to variations in toxicity. In a recent study, it was demonstrated that the formation of a humic acid corona on polystyrene nano-plastic particles[17] alleviates the toxicity of nano-plastic particles to the aquatic crustacean *Daphnia magna*.

In this study, molecular dynamics (MD) simulations are performed to investigate the surface interactions between NOM molecules and PS nano-plastics in an aqueous environment of both fresh and saltwater. The pH of water in rivers and lakes generally ranges between 5 and 9, whereas ocean water[18] averages closer to 8.2. Hence, the simulations are considered at three different pH ranges: acidic (pH 4), neutral (pH 7), and basic (pH 9) aqueous environments. Humic acids are the main constituents of NOM, and the Temple-Northeastern-Birmingham (TNB) model has been utilized to mimic NOM in our simulations due to its similarity in composition to humic acid.[19–21] Our main aim has been to elucidate the processes at the atomistic level that govern the interactions of NOM molecules with the charged nano-plastic surfaces, hence providing insight into the binding affinities and surface complexation with the nano-plastics. This is crucial in understanding the formation of eco-corona and its stability in different aqueous environments.

2. Materials and methods

2.1 Experimental

2.1.1 Zeta potential measurements. Polystyrene particles were purchased from Applied Nanoparticles, a nanotech engineering company. According to the supplier, polystyrene nanoparticles (NPs) have gold as a core coated with silica and polystyrene (Au@SiO_2@PS NPs). The polystyrene layer contains carboxylic functional groups. The average diameter of the polystyrene beads measured by TEM is 80 nm. The measurements of zeta potentials were performed using a Malvern Nano Zetasizer in backscattering mode (173°) with DTS1070 folded capillary cells. The measured electrophoretic mobility was converted to zeta potential by using Smoluchowski theory, which is used by default in the instrument.

2.2 Simulations

2.2.1 Simulation model. The polystyrene nano-plastic was modelled as a slab and was generated by combining 44 chains of atactic polystyrene of different lengths using the tool packmol-20.01.[22] The hydrocarbons on the polystyrene chains were represented in the united atom model. The generated slab was then energy minimized and equilibrated well to avoid bad contacts and obtain structural integrity. The

dimensions of the obtained slab were 4.8 × 2.8 × 4.8 nm^3 in length, width, and height along *X*, *Y*, and *Z*-directions, respectively. Over 70 carboxylate groups were ascribed to the PS-slab by distributing them randomly over the surface using the tool Avogadro[23] and then equilibrated well to minimize the potential energy of the system. The molecular structure of the TNB molecule comprises three carboxylic (R-COOH) groups, three carbonyls (R-CO), two phenolic (R-OH) groups, two amines (R-NH_2), and four other alcohol groups and has a chemical composition of ($C_{36}H_{40}O_{16}N_2$).[24] The carboxylated groups of the TNB molecule were deprotonated in the pH range of 4–9 (pK_a = 4–5), whereas the phenolic (pK_a = 9) and amine groups (pK_a = 4.6) were in a protonated state.[25]

Five such molecules of TNB were distributed randomly over the simulation box of size 9 × 9 × 9 nm^3, with the PS-slab being at its center, as shown in Fig. 1. The simulation box was then filled with the water molecules using the TIP4P model explicitly. In total, six different systems were prepared for pH 4, 7, and 9 at 0 M and 0.5 M NaCl concentrations. The pH 4 system resembled the case in which 15% of the carboxylate groups of the PS-slab are deprotonated (11 COO^-), pH 7 was the one with 60% (42 COO^-), and pH 9 with 98% (69 COO^-), respectively.[26] In all these systems, the carboxylate groups of the TNB molecules were deprotonated (3 COO^-), whereas the amines (–NH_2) and phenolic groups (–OH) always remain electrically neutral in the pH range of 4–9.[27] The required number of sodium ions was added to the box wherever necessary by replacing the solvent molecules to maintain the charge neutrality of the simulation box.

2.2.2 Computational details. The required topology files corresponding to the PS-slab and TNB molecules were prepared to define all the bonds, angles, dihedrals, masses, and charges of each atom, and their charge groups were prepared using the CHARMM GUI interface.[28] All of our MD simulations were performed using the GROMACS-2021.5 package,[29] and CHARMM force field[30,31] was used to model the interatomic interactions. To replicate an infinite system, periodic boundary conditions were implemented in all three directions of the simulation box. All simulations were performed at a temperature of T = 300 K and a pressure of P = 1 bar. The systems were first well equilibrated in an NVT ensemble for t = 100 ps, and then final production runs were performed using an NPT ensemble for t = 100 ns. A Berendsen coupling thermostat and barostat[32] with a relaxation time of τ = 0.1 ps are used for temperature control and τ = 2.0 ps for pressure control. The van der Waals forces are calculated using a smooth cut-off of 8–10 Å. The force constant was set to 40 kcal $Å^{-2}$ mol^{-1}. To hold the PS-slab at the center of the box, the carbon atoms of the polystyrene backbone were restrained, and the surface carboxylate groups were allowed to respond as per the dynamics of the system. All the electrostatic interactions carried out in this study are evaluated using a 'particle–particle particle–mesh' Ewald solver[33] with a grid spacing of 1 Å. The equations of motions were integrated using a time step size of 2 fs.

3. Results and discussion

3.1 Interactions among TNB molecules and polystyrene nano-plastic

3.1.1 Adsorption of TNB organic matter. The interaction of NOM molecules is strongly influenced by the surface charge density of nano-plastics. With an increase in the pH of the aqueous environment surrounding the nano-plastics, the surface carboxylate groups are deprotonated and ascribe a negative charge to it with a varying charge density.

To investigate the interactions between the TNB molecules and nano-plastic (PS-slab), the radial distribution function

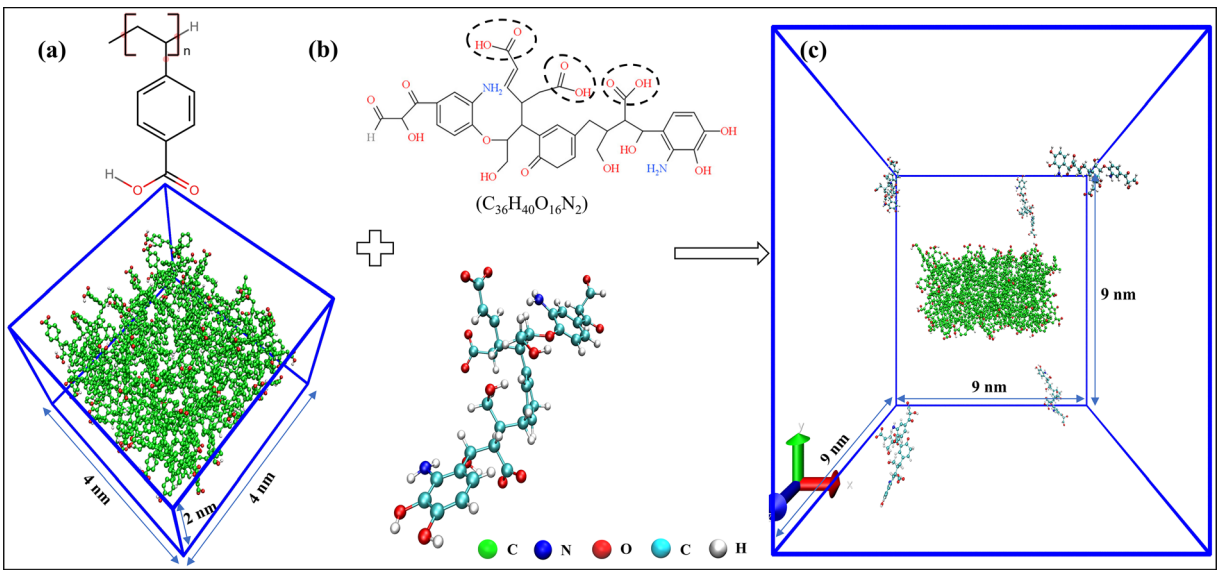

Fig. 1 Snapshots of the simulation models (a) PS-slab; (b) TNB molecule; (c) representative unit of a simulation cell depicting the starting structure of MD simulation, water molecules are not shown here for visual clarity.

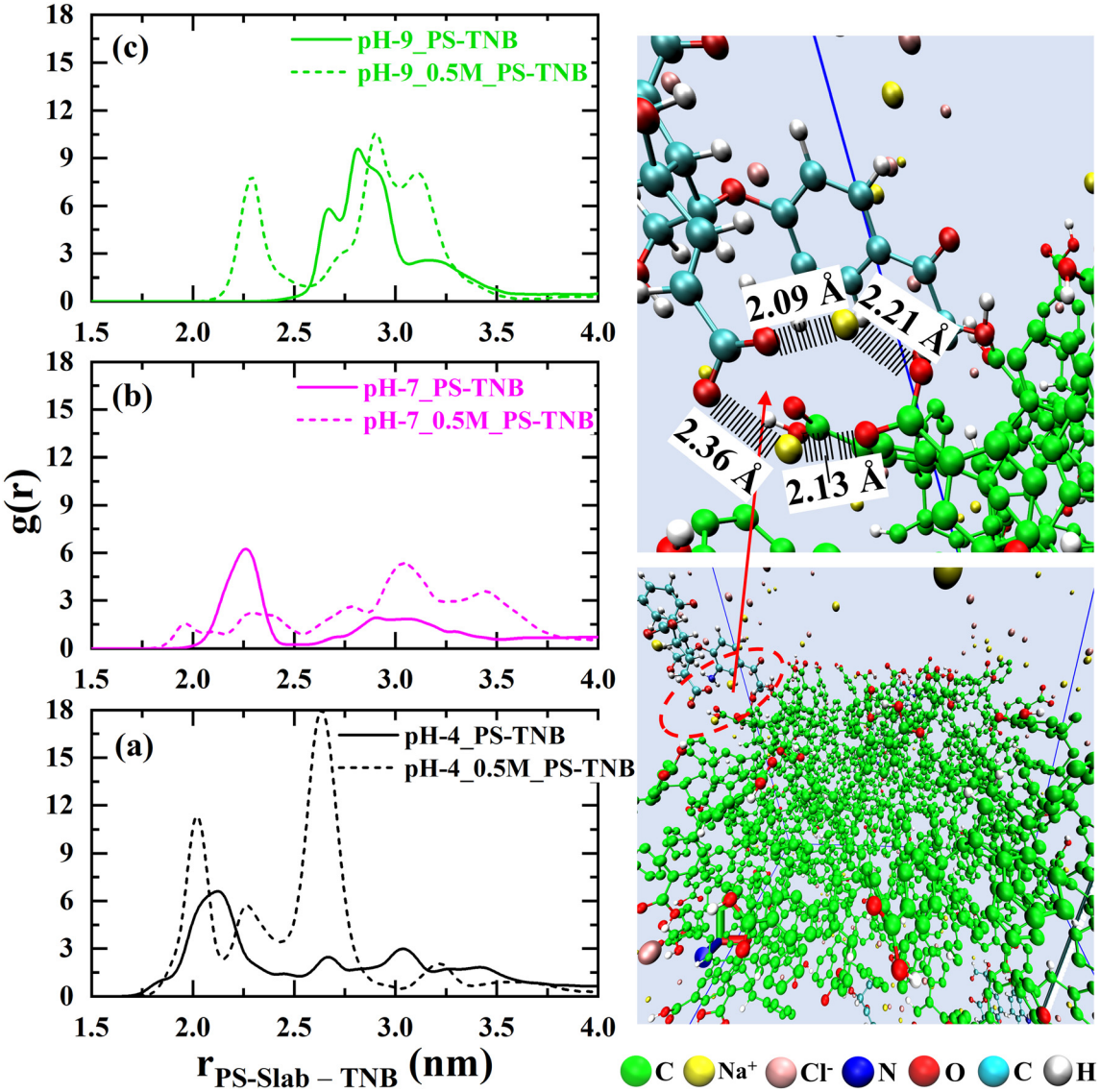

Fig. 2 Radial distribution profiles of TNB molecules adsorbed on the surface of the PS-slab in an aqueous environment of fresh and salt (0.5 M NaCl) water at various pH conditions; (a) pH-4; (b) pH-7; (c) pH-9. The inset represents the Na^+ ion-mediated interaction between the carboxylate groups of TNB molecule and PS–COOH nano-plastic.

(RDF) was calculated as a function of TNB molecules, as displayed in Fig. 2. This gives us an insight into the behaviour of natural organic matter near the surface of nano-plastics under different aquatic conditions. A significant difference in interactions of the TNB molecules with the PS-slab is observed for the systems at pH values of 4, 7, and 9 in fresh as well as in saltwater.

From Fig. 2(a), there is a clear trend exhibiting that the system with pH 4 has a higher probability of TNB molecules remaining close (1.5 nm) to the surface of the PS-slab as compared to other systems considered in this study. This is due to the van der Waals attractive force induced among the aromatic rings that are present in both PS-slab and the TNB molecules. Although coulombic repulsive interactions exist between the TNB molecules and PS-slab due to the negatively charged carboxylic groups, the contribution of van der Waals forces becomes large due to the significant number of aromatic rings present in both TNB and PS-slab as compared to the number of negatively charged carboxylic groups. With the addition of 0.5 M of NaCl electrolyte, the accumulation of TNB molecules increased in the vicinity of the PS-slab. This enhanced accumulation can be inferred from the counter-ion (Na^+) induced attractive interaction between the negatively charged carboxylate groups of TNB molecules and PS-slab, bringing the TNB molecules closer to the surface of the PS-slab.

At pH 7 (Fig. 2(b)), TNB molecules exhibited a relatively weak interaction as to all other systems studied. A shift in the peak ($\approx$ 2 nm) was observed for the distribution of TNB molecules elucidating the coulombic repulsive interactions arising among the negatively charged carboxylate groups. Hence, the molecules are pushed away from the surface of

the PS-slab as compared to the system at pH 4. However, with the addition of 0.5 M NaCl electrolyte, a close shift (≈ 1.5 nm) in the distribution is observed, exhibiting a counter-ion-induced relatively weak attractive interaction.

At pH 9 (Fig. 2(c)), the TNB molecules exhibit a moderate interaction with the PS-slab as to the systems studied at pH 4 & 7. The TNB molecules are further pushed away (≈ 2.5 nm) from the surface of the PS-slab as to the systems at pH 4 & 7. This is due to an increase in the coulombic repulsive interactions between TNB molecules and PS-slab as the number of charged carboxylate groups increases with an increase in pH. However, in saltwater, counter-ion-induced attractive interactions bring the TNB molecules closer (≈ 2 nm) to the surface of the PS-slab.

From these interaction profiles, it can be inferred that TNB molecules are less likely to adsorb onto the PS-slab at high pH conditions, *i.e.*, if it carries a higher surface charge density. The coulombic repulsive interactions among the deprotonated carboxylate groups take precedence over the van der Waals attractive interactions with the aromatic rings of PS and TNB molecules, leading to less adsorptivity. Also, Na^+ ion bridging takes place as the ions interact with negatively charged carboxylate groups of TNB and PS-slab, thereby bringing TNB molecules closer to the interface of nano-plastics in saltwater.

3.1.2 Interactions among TNB molecules. The interactions among the TNB molecules at different pH conditions of aquatic environments are analysed using the RDF profiles, as shown in Fig. 3. The aggregation among the TNB molecules in the aquatic solution of pH-4 and 9 (Fig. 3(a) and (c)) in the presence of 0.5 M NaCl is higher as to the case of 0 M NaCl. The observed strong association among the TNB molecules can be ascribed to the Na^+ ion-mediated attractive interactions induced among the negatively charged carboxylate groups of the TNB molecules. However, at pH 7 (Fig. 3(b)) in 0.5 M NaCl, the aggregation among the TNB molecules is weaker as compared to 0 M NaCl. Hence, at pH 7, most of the TNB molecules remain in solution as individual entities and are also less likely to be observed at the interface of the PS-slab (Fig. 2(b)). Whereas, at pH 4 & 9 with 0.5 M NaCl, there is a strong association among the TNB molecules (Fig. 2(a) and (c)) observed at the interface of PS-slab.

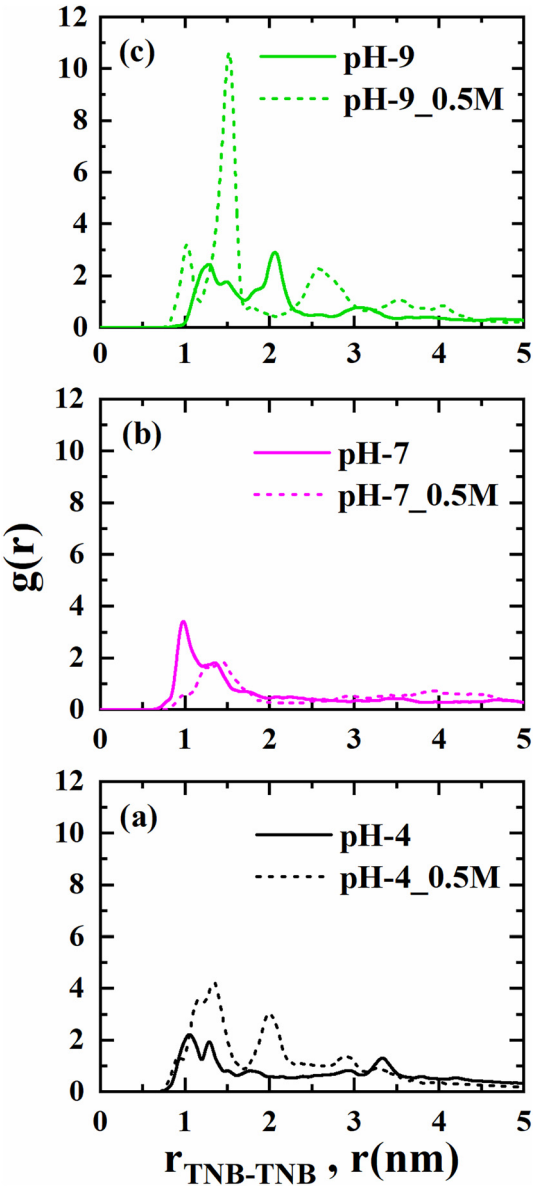

Fig. 3 Radial distribution profiles representing the interactions among TNB molecules in fresh and salt (0.5 M NaCl) water at various pH conditions; (a) pH-4; (b) pH-7; (c) pH-9.

3.2 Counter-ion condensation

To investigate the affinity of Na^+ ions in relation to the surface charge density of the PS-slab in various aquatic environments, the number density distribution of Na^+ ions starting radially outward from the center of the PS-slab with a bin width of 0.05 nm is calculated and plotted as shown in Fig. 4. Comparing the RDF plots, the Na^+ ions show stronger interaction with the PS-slab with an increase in the pH of the aqueous solution. The density of Na^+ ions is lower at the interface of the PS-slab at pH 4 and increases with an increase in its surface charge density[34] at pH 7 & 9. The increase in the condensation of Na^+ ions is due to counterbalancing the negative charge of the deprotonated carboxylate groups at increasing pH conditions of aquatic solution.

3.3 Dynamic properties of water

3.3.1 Water density distribution. Fig. 5 shows the number density distribution of oxygen atoms of water molecules in the vicinity of PS-slab starting from its geometric center with a bin width of 0.05 nm varying linearly across the simulation box in the *X*-direction with limitations along *Y* & *Z*-direction. An increase in the density of water molecules with an increase in the pH of the aquatic environment is observed. The increase in the density of water molecules at the

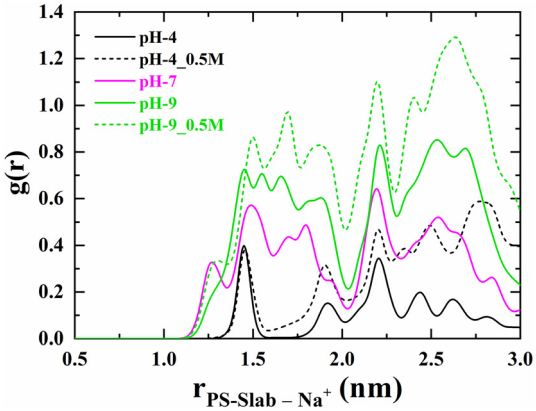

Fig. 4 Radial number density distribution profiles for sodium ions adsorbed on the interface of PS-slab at pH-4, pH-4_0.5 M, pH-7, pH-9 & pH-9_0.5 M.

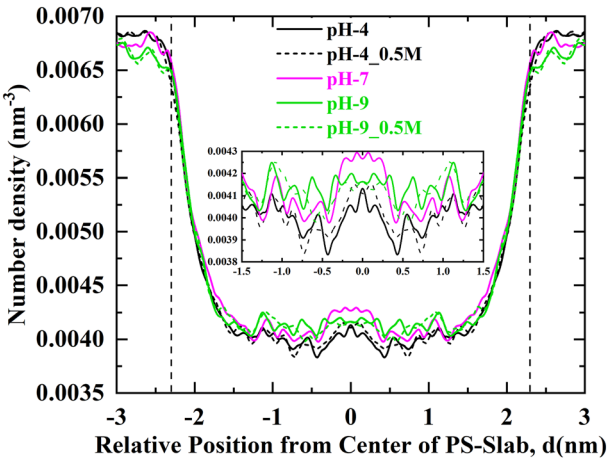

Fig. 5 Number density profiles of water molecules around the PS-slab at pH-4, pH-7, and pH-9 at 0 M and 0.5 M NaCl. The dashed lines represent the reference positions for the PS-slab geometric interface along the *X*-axis.

geometric interface of PS-slab can be ascribed to the hydration of negatively charged carboxylate groups and is also due to the hydrated Na^+ ions condensed onto the interface (Fig. 4), which brings more water molecules to the interface.[35] The strong hydration layer observed at the interface of nano-plastics at pH 7 & 9 is also one of the reasons that keep the TNB molecules away from the vicinity of its interface. Hence, the reduction in the distribution of TNB molecules (RDF profiles, Fig. 2(b) and (c)) at higher surface charge densities of the PS-slab.

3.3.2 Hydrogen bonding interactions. Water molecules can establish hydrogen bonds with the negatively charged sites of the PS-slab (ionized carboxylate groups). Hydrogen bonding between the PS-slab and the surrounding water molecules was calculated to get an insight into the structure of water molecules at its interface in different pH conditions. The following criteria were adopted for calculating the formation of hydrogen bond: the distance between the donor ($O_{Carboxylate}$) and acceptor (H_{Water}) is less than 3.5 Å, the distance between the oxygen of the acceptor molecule (O_{Water}) and hydrogen of the donor molecule ($H_{Carboxylate}$) is not more than 2.4 Å, and hydrogen ($H_{Carboxylate}$)–donor ($O_{Carboxylate}$)–acceptor (H_{Water}) angle of below 30°.

Fig. 6(a) represents the average number of hydrogen bonds (h-bonds) formed at the interface of the PS-slab between the carboxylate groups of polystyrene and the surrounding water molecules. The number of h-bonds increased with an increase in the pH of the aqueous solution. This can be ascribed to the polarizability of water molecules[35,36] induced by the negatively charged carboxylate groups on the surface of the PS-slab. However, with the addition of 0.5 M NaCl electrolyte, a reduction in the number of h-bonds was observed, which can be inferred as the distortion in the structure of the h-bonds[37] between the carboxylate groups and the surrounding water molecules due to the Na^+ ions.

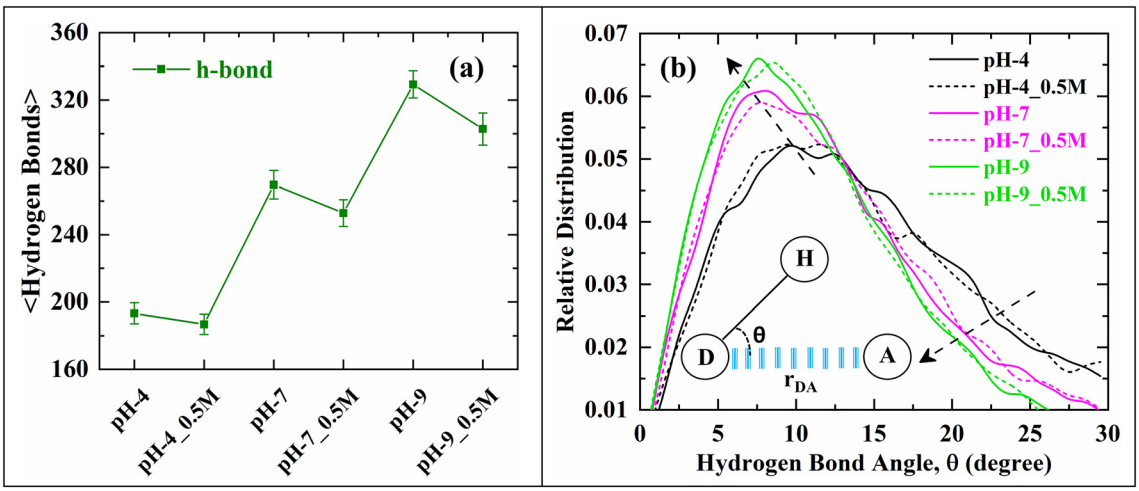

Fig. 6 (a) The average number of hydrogen bonds with error bars formed at the PS-slab–water interface at various pH conditions; (b) hydrogen-bond angle distributions observed at the PS-slab–water geometrical interface.

Fig. 6(b) represents the strength of the h-bond interactions existing between the carboxylate groups of PS and water molecules. We observed that with an increase in the pH of the aqueous solution, the strength of the h-bonds increased, and the peak shifted to lower angles. The relative distribution representing the distance between the donor ($O_{Carboxylate}$) and acceptor (H_{Water}) distance is reported in Fig. S2 of ESI.† This increase in strength is due to the high surface charge associated with the PS-slab, which in turn polarises more surrounding water molecules resulting in the alignment of water molecules leading to a more structured network of water molecules at the geometric interface of the PS-slab with an increase in pH of the aqueous environment. An ordered network structure of water molecules leads to the accommodation of a higher number of water molecules at the interface of PS-slab and hence the observed increase in their density (Fig. 5) at the interface resulting in a strong hydration layer.

3.4 Electrostatic potential distribution

The surface charge on nano-plastics plays a major role in driving the adsorptivity of organic matter molecules onto their surface. Surface potential is a measure of quantifying the surface charge on the nano-plastics at different aquatic conditions. Hence, the surface potential of the PS-slab was analyzed for the systems at different pH intervals considered in this study, as shown in Fig. 7. The electrostatic potential is calculated by integrating the charge density on *YZ*-plane across the simulation box along the *X*-direction. The electrostatic potential is observed to be negative with increasing pH of the surrounding aquatic environment of PS-slab. The surface potential is large and negative at pH 9 (1 V), which can be attributed to the greater number of deprotonated carboxylate groups of PS-slab contributing to its negative charge. However, with the addition of 0.5 M NaCl electrolyte, the potential has been reduced considerably to 0.6 V. This significant reduction in the negative potential is due to the screening of its surface charge by Na^+ ions that are adsorbed onto the interface of PS-slab (Fig. 4). The observed inferences are consistent with the idea of screening of surface charge with enhanced condensation of Na^+ ions,[35,38,39] and consequently a decrease in Debye screening length. A similar trend is observed for the surface potentials calculated for PS-slab at pH-4 and pH-7 at 0 M and 0.5 M NaCl.

3.4.1 Zeta potential measurements. The PS–COOH nanoparticles collected from the wetland mesocosms are analysed for surface charge density at different pH intervals with the potential at real particle surfaces using the Zetasizer. All measurements are performed with 1 mM NaCl as the background electrolyte. Zeta potential values gradually decrease with increasing pH value (Fig. 8) of the aqueous environment of PS–COOH nanoparticles. The values are found to be relatively negative, ranging from −42 mV to −56 mV, in the pH range of 3 to 11. This corresponds to the pH range, at which the surface charge density of PS–COOH nanoparticles increases due to the ionized (negatively charged oxygen) carboxylated groups, contributing to the long-range electrostatic stabilization of these dispersions.

The zeta potentials inferred from the experiments correlate well with the trends of the surface potentials (Fig. 7, pH 4, 7 & 9) measured from the simulations qualitatively, thus depicting negative surface potential as a result of increased surface charge density of PS–COOH due to the ionized carboxylate groups of its surface with an increase in pH of the aqueous environment.

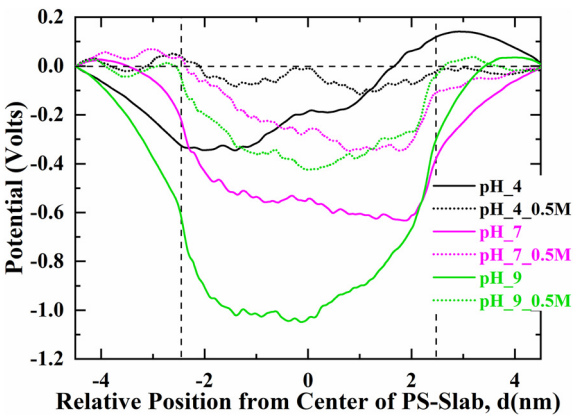

Fig. 7 Electrostatic potential profiles for the PS-slab at different pH (4, 7, and 9) values. The dashed lines represent the interface of PS-slab in the *X*-direction.

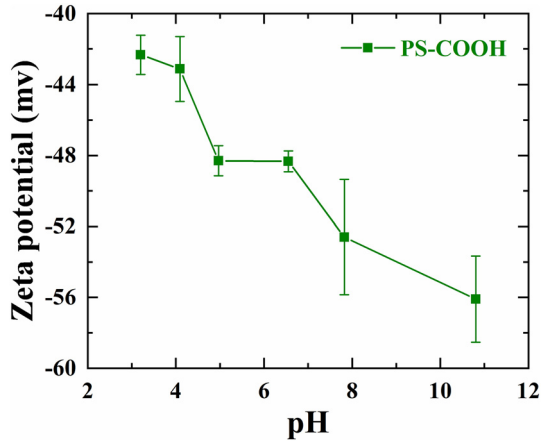

Fig. 8 The zeta potentials corresponding to the carboxylated polystyrene latex nanoparticles at different pH conditions of the aquatic environment.

4. Conclusions

In conclusion, the simulations have given us an insight into the charge of PS-slab playing a major role in influencing the adsorption behaviour of TNB molecules, Na^+ ions, and water molecules onto its interface. We show that the development of eco-corona at the interface of PS-slab is higher in a system at pH-4 with 0.5 M NaCl electrolyte and lower at pH-7 with 0.5 M NaCl. We also show that Na^+ ions exhibit a strong affinity towards the interface of PS-slab with an increase in pH of the aquatic solution both in fresh and saltwater, which in turn affects the hydrophilicity of PS nano-plastic. A structured network of water molecules has also been observed with an increase in pH of the aqueous solution, thereby accumulating a greater number of water molecules at the interface of PS-slab, resulting in a strong hydration layer, keeping the TNB molecules away from the vicinity of its interface. The trends in the surface potentials calculated over different charge densities of the PS-slab at different aquatic conditions are validated with the zeta potential measurements of samples from wetland mesocosms.

Therefore, these interactions provide an insight into the fate of nano-plastics in controlling the binding/adsorption/accumulation of organic molecules/ions/water molecules on the surface of nano-plastics in various aquatic conditions. Therefore, the results of this study are useful for providing, at a molecular level, a detailed understanding of eco-corona development around the nano-plastics in an ecosystem. Although our simulation results do not illustrate toxicity, however, the binding mechanisms leading to eco-corona around the nano-plastic at different pH conditions of the aquatic environment are relevant for evaluating and understanding the toxicity of these nano-plastics to living organisms. The interactions between carboxylated nano-plastics and dissolved organic matter can be complex and depend on factors, such as ionic strength, temperature, salinity, and the concentration of the organic matter, in addition to the pH of the aquatic environment. The interactions between the PS-slab and TNB can also be affected by the presence of other molecules, ions, or inorganic colloids in the solution. However, the representative model used in this study can simplify the understanding of the interactions governing the development of eco-corona. The future investigations of this study can further be extended by including different salts and inorganic colloids in aquatic environments.

Conflicts of interest

There are no conflicts of interest to declare.

Acknowledgements

The authors would like to acknowledge Mistra (The Swedish Foundation for Strategic Environmental Research) for funding (DIA 2013/48) of this work under the Mistra Environmental Nanosafety project. We are grateful to Dr. Rakesh Vaiwala and Prof. Lars-Anders Hansson, Franca Stabile, and Mikael Ekvall for their helpful inputs regarding the work. We also thank the Swedish National Infrastructure for Computing (SNIC) for providing us with the computational time.

References

1 R. Mohammad-Rezaei, B. Massoumi, M. Abbasian and M. Jaymand, *J. Polym. Res.*, 2018, **25**(4), 1572–8935.
2 S. Moulay, *Polym.-Plast. Technol. Eng.*, 2018, **57**, 1045–1092.
3 F. M. Windsor, I. Durance, A. A. Horton, R. C. Thompson, C. R. Tyler and S. J. Ormerod, *Global Change Biol.*, 2019, **25**, 1207–1221.
4 K. Kik, B. Bukowska and P. Sicińska, *Environ. Pollut.*, 2020, **262**, 114297.
5 S. Lambert and M. Wagner, *Chemosphere*, 2016, **145**, 265–268.
6 H. K. Imhof, J. Schmid, R. Niessner, N. P. Ivleva and C. Laforsch, *Limnol. Oceanogr.: Methods*, 2012, **10**, 524–537.
7 K. Mattsson, E. V. Johnson, A. Malmendal, S. Linse, L. A. Hansson and T. Cedervall, *Sci. Rep.*, 2017, **7**, 1–7.
8 K. Mattsson, L. A. Hansson and T. Cedervall, *Environ. Sci.: Processes Impacts*, 2015, **17**, 1712–1721.
9 E. M. F. Kallenbach, E. S. Rødland, N. T. Buenaventura and R. Hurley, *Microplastics in Terrestrial and Freshwater Environments*, 2022, pp. 87–130.
10 I. Kögel-Knabner, *Soil Biol. Biochem.*, 2002, **34**, 139–162.
11 Z. Parsi, N. Hartog, T. Górecki and J. Poerschmann, *J. Anal. Appl. Pyrolysis*, 2007, **79**, 9–15.
12 R. Frankel, M. T. Ekvall, E. Kelpsiene, L. A. Hansson and T. Cedervall, *Environ. Sci.: Nano*, 2020, **7**, 1518–1524.
13 M. T. Ekvall, J. Hedberg, I. Odnevall Wallinder, A. Malmendal, L. A. Hansson and T. Cedervall, *Sci. Rep.*, 2021, **11**, 10784.
14 M. Shams, I. Alam and I. Chowdhury, *Water Res.*, 2021, **197**, 117066.
15 J. Saavedra, S. Stoll and V. I. Slaveykova, *Environ. Pollut.*, 2019, **252**, 715–722.
16 C. L. Schultz, S. Bart, E. Lahive and D. J. Spurgeon, *Environ. Sci. Technol.*, 2021, **55**, 6065–6075.
17 O. O. Fadare, B. Wan, L. H. Guo, Y. Xin, W. Qin and Y. Yang, *Environ. Sci.: Nano*, 2019, **6**, 1466–1477.
18 T. I. Moiseenko, M. I. Dinu, N. A. Gashkina, V. Jones, V. Y. Khoroshavin and T. A. Kremleva, *Environ. Res. Lett.*, 2018, **13**, 105007.
19 E. Iskrenova-Tchoukova, A. G. Kalinichev and R. James Kirkpatrick, *Langmuir*, 2020, **26**, 15909–15919.
20 A. G. Kalinichev, *Pure Appl. Chem.*, 2013, **85**, 149–158.
21 A. G. Kalinichev and R. J. Kirkpatrick, *Eurasian J. Soil Sci.*, 2007, **58**, 909–917.
22 L. Martinez, R. Andrade, E. G. Birgin and J. M. Martínez, *J. Comput. Chem.*, 2009, **30**, 2157–2164.
23 M. D. Hanwell, D. E. Curtis, D. C. Lonie, T. Vandermeerschd, E. Zurek and G. R. Hutchison, *Aust. J. Chem.*, 2012, **4**, 1–17.
24 X. Wu, Y. Xia, L. Yuan, K. Xia, Y. Jiang, N. Li and X. He, *Water*, 2020, **12**, 3200.

25 Y. Ai, C. Zhao, L. Sun, X. Wang and L. Liang, *Sci. Total Environ.*, 2020, **702**, 135072.
26 S. F. Schulz, T. Gisler, M. Borkovec and H. Sticher, *J. Colloid Interface Sci.*, 1994, **164**, 88–98.
27 J. D. Ritchie and E. Michael Perdue, *Geochim. Cosmochim. Acta*, 2003, **67**, 85–96.
28 E. L. M. Lundborg, *J. Phys. Chem. B*, 2015, **3**, 810–823.
29 M. J. Abraham, D. van der Spoel, E. Lindahl, B. Hess and the GROMACS development team, DOI: **10.5281/ZENODO.5850051**.
30 W. L. Jorgensen and D. S. Maxwell, *J. Am. Chem. Soc.*, 1996, **118**, 11225–11236.
31 W. L. Jorgensen, *J. Am. Chem. Soc.*, 1988, **110**, 11225–11236.
32 H. J. C. Berendsen, J. P. M. Postma, W. F. Van Gunsteren, A. Dinola and J. R. Haak, *J. Chem. Phys.*, 1984, **81**, 3684–3690.
33 U. Essmann, L. Perera, M. L. Berkowitz, T. Darden, H. Lee and L. G. Pedersen, *J. Chem. Phys.*, 1995, **103**, 8577–8593.
34 A. Clavier, F. Carnal and S. Stoll, *J. Phys. Chem. B*, 2016, **120**, 7988–7997.
35 P. Rama and Z. Abbas, *Phys. Chem. Chem. Phys.*, 2022, **24**, 3713–3721.
36 S. Ong, X. Zhao and K. B. Eisenthal, *Chem. Phys. Lett.*, 1992, **191**, 327–335.
37 P. A. Covert, K. C. Jena and D. K. Hore, *J. Phys. Chem. Lett.*, 2014, **5**, 143–148.
38 P. Rama, A. R. Bhattacharyya, R. Bandyopadhyaya and A. S. Panwar, *J. Phys. Chem. C*, 2018, **122**, 9619–9631.
39 P. Rama, A. R. Bhattacharyya, R. Bandyopadhyaya and A. S. Panwar, *J. Phys. Chem. C*, 2019, **123**, 1974–1986.